A Polar Magnetic Paleopole Associated with Apollinaris Patera, Mars

Benoit Langlais [a,b] and Michael Purucker [c]

[a] *CNRS, Université de Nantes, Nantes Atlantique Universités, Laboratoire de Planétologie et de Géodynamique,*

UMR 6112, 2 rue de la Houssinière,

F-44000 Nantes, France

phone: +33 (0) 252 125 497; fax: +33 (0) 251 125 268,

email: benoit.langlais@univ-nantes.fr

[b] *NAS/NRC at Planetary Geodynamics Lab,*

NASA/GSFC,

Greenbelt MD 20771, USA

[c] *Raytheon at Planetary Geodynamics Branch,*

code 698, NASA/GSFC,

Greenbelt MD 20771, USA

email: purucker@geomag.gsfc.nasa.gov

Abstract

A Martian paleomagnetic pole is calculated from a magnetic anomaly associated with the late Noachian age (and older) volcano Apollinaris Patera. This isolated

Preprint submitted to Elsevier Science *7 March 2006*

volcano, located near the crustal dichotomy boundary at the Martian equator, has a correlative gravity anomaly, and was likely active for more than 10^7 years. It is one of the only volcanoes on Mars known to have a substantial magnetic anomaly associated with it, and one of the only examples of correlative magnetic and gravity sources. Magnetic directions calculated using either low- or high-altitude data, and single or multiple equivalent source dipoles, are nearly horizontal and southward directed. Assuming a single dipolar source magnetization, the preferred paleopole is at 65°S, 59°E. Assuming a larger magnetized area leads to a cluster of paleopoles near 88°S, 99°E. This paleopole is very close to the current rotational pole, and very different from previously calculated paleopoles. Our preferred interpretation is that the Apollinaris Patera magnetization was acquired near the end of the life of the Martian dynamo, and that subsequent polar wander was minimal.

Key words: Mars; Magnetic Fields; Paleopoles; Apollinaris Patera;

1 Introduction — Geological setting

When compared to the Earth, Mars possesses a strong remanent lithospheric field. It has been discovered by the Mars Global Surveyor (MGS) mission. The present magnetic field of Mars likely is the signature of an ancient Earth-like geodynamo magnetic field (Stevenson, 2001). It can be very intense locally, reaching 1500 nT at 100 km over Terra Cimmeria and Terra Sirenum. The strength of this magnetic field may be due to multiple factors, including a thick cool lithosphere with a high magnetic material content, and a strong paleodynamo.

Several global models of the present remanent field have been developed in order to better understand the ancient magnetic field of Mars. Early studies directly utilized the magnetic measurements (Acuña *et al.*, 1999; Connerney *et al.*, 2001). The latter created a map of the magnetic field based on MO measurements. Only the median value in each $1 \times 1°$ bin was retained. Global modeling approaches, based on Spherical Harmonics Analysis (SHA) (Cain *et al.*, 2003; Arkani-Hamed, 2004) or Equivalent Source Dipoles (ESD) (Purucker *et al.*, 2000; Langlais *et al.*, 2004) have also been employed. The SHA is commonly used to model the Earth's magnetic field (Gauss, 1839), in particular its large core field. The ESD is generally used when considering magnetic field of lithospheric origin (Langel and Hinze, 1998).

Both techniques provide similar description of the magnetic field at satellite altitude: the Martian magnetic anomalies are hemispherically distributed. The largest anomalies are one or two orders of magnitude larger than what is thought to be the terrestrial remanent magnetic field, reaching some 200 nT at 400 km altitude (Connerney *et al.*, 2004). This is to be compared to some 20 nT on the Earth at similar altitudes (Maus *et al.*, 2002). Both SHA and ESD techniques agree on the magnitude of the magnetic field at the surface level: it may well exceed 10000 nT (Langlais *et al.*, 2004). Measurable magnetic fields (at satellite altitude) are mostly found South of the crustal dichotomy, a boundary of enigmatic origin between the Northern lowlands and the Southern highlands (Zuber, 2001). Mars also possesses large areas where the magnetic field is weak, or unmeasurable. This is the case over the largest impact craters (Hellas, Argyre, Isidis), and also above the largest volcanoes (Tharsis, Elysium, Olympus). A simple scenario can explain these observations: an Earth-like Martian dynamo was active during the first stages of the planet evolution; it stopped at a certain epoch, and was not active when destructive events (impacts, volcanic eruptions) took place; the remanent magnetic field, if any, was thus locally erased by thermal or shock demagnetization (Hood *et al.*, 2003). Another scenario, in which a dynamo started after these catastrophic events (Schubert *et al.*, 2000), seems unlikely, as the strongest magnetic anomalies lies below terranes that seem to be older than the impacts and the volcanoes (Frey, 2004).

Global models of the magnetization have also been developed, either jointly with models of the magnetic fields (Langlais *et al.*, 2004), or as magnetization only models (Arkani-Hamed, 2002; Whaler and Purucker, 2005). These models eliminate non-uniqueness either through the norm that they minimize (Langlais *et al.*, 2004; Whaler and Purucker, 2005) or through the specification of a dipolar field and paleopole location (Arkani-Hamed, 2002). Albeit non unique, the derived magnetization distributions described above may be seen as what could be the direction and the contrasts of the actual magnetization of the Martian lithosphere. Parker (2003) estimated what would be the minimum magnetization capable of producing the high intensity magnetic field observed in the South hemisphere. Assuming a 50-km thick layer, the magnetization must be at least 4.76 A/m. This is very consistent with the model of (Connerney *et al.*, 1999), who reported a +/- 20 A/m for 30-km thick contiguous magnetized plates. Langlais *et al.* (2004) gave a +/- 12 A/m range for a 40-km thick layer, while Nimmo and Gilmore (2001) found $\simeq$40 A/m for a 10-km thick layer.

Several studies have attempted to delineate paleopoles. One approach is to use 'isolated' magnetic anomalies, and apply forward modeling techniques. An unique solution is not guaranteed in this approach, and interactions with adjacent anomalies are handled subjectively. Hood and Zakharian (2001) modeled two isolated magnetic anomalies, located near the North Pole. The associated paleopole they computed is located near 45°N, 225°E. Using 10 isolated magnetic anomalies, Arkani-Hamed (2001) found that 7 out of 10 paleopoles formed a cluster around 25°N, 230°E. In another study, (Arkani-Hamed and Boutin, 2004) found a dual clustering of paleopoles, based on the analysis of nine magnetic anomalies. All these studies lead to two observations: none of the computed paleopoles coincide with the actual rotation axis, and contiguous paleopoles may be of reversed polarity. This can be explained by a reversing Martian dynamo, plus polar wander between the present and the epoch when the magnetized bodies acquired their magnetization.

These paleopoles are based on local approaches. Global approaches have placed these local results in context, and can be used to assess some measure of their uncertainty. Langlais *et al.* (2004) interpolated magnetization directions between the equivalent source dipoles so that the sources would be located at the same locations as those described by Arkani-Hamed (2001). The inclinations they found are within 10° of the ones given by (Arkani-Hamed, 2001), in seven out of ten cases. The three remaining are different by less than 30°. Whaler and Purucker (2005) found that 5 out of 10 paleopoles fell within 30°, and that the average separation was 35°.

It is however difficult to interpret these results. The location of the paleopole strongly relies on the geometry and the location of the magnetized source, as well as on the data availability and the method used. Arkani-Hamed and Boutin (2004) compared their results to previous studies in their Table 1. For instance, their anomaly 5 gives two distinct paleopoles, although its prismatic source is located at almost the same location. Unique solution does not exist, unless the location of the source can be *a priori* set.

At least one volcano is not correlated with a null magnetic field. This is Apollinaris Patera (9.3°S, 174.4°E). This volcanic edifice rises about 5 km above the surrounding terranes. Its shape is a 200 km-wide dome, with a 75 km-wide caldera on its summit (Figure 1a). Its history consists of at least two distinct phases: a first one explosive, forming the main edifice; and a second one effusive, forming the southern flows (Robinson *et al.*, 1993). According to recent crater counts, its active period ended early in the Martian history at about 3.71 Ga ago (Werner , 2005). This volcano is also quite isolated. In contrast with other volcanoes, it does not lie along a fault zone, nor it is aligned with other volcanoes. This volcano presents a strong gravity anomaly, as revealed by the model of Lemoine *et al.* (2001). A map of the gravity anomaly is shown on Figure 1b. The location of the maximum gravity anomaly is -8.75°S, 174.5°E, which is almost the location of the top of the Patera.

`Figure 1`

In this paper, we present a summary of the measurements acquired near the location of this volcano. The considered area is between 160 and 190° East longitude, and -25 and +5° North latitude. We then describe the modeling method. We finally present the results of the modeling, and discuss their implications in terms of paleopole locations.

2 Magnetic Measurements

Mars Global Surveyor was launched on November 7th, 1996, and reached Mars orbit on September 11th, 1997. We herein briefly recall the four mission phases.

A review of the mission characteristics and main results can be found in Albee *et al.* (2001). The first AeroBraking (AB-1) phase was followed by a Science Phasing Orbit (SPO), then a second AeroBraking (AB-2) phase, and finally the Mapping Orbit (MO) cycles. Because of this configuration measurements were acquired at both low (down to 90 km) and high (near 400 km) altitudes. There is thus a dual altitude coverage, even if the lowest one is far from being complete. In this study we considered measurements from the AB-1 phase below 250-km altitude (between days 322 of 1997 and day 22 of 1998), as well as night-side measurements from the MO phase (between days 67 of 1999 and 262 of 2001). Measurements are shown on Figures 2 and 3 for the AB-1 and MO phases, respectively.

`Figure 2`

`Figure 3`

It is crucial to test both the validity and the stability of the magnetic measurements because the relationship between the solution and the observations is not unique. Given the large amount of measurements, it is possible to keep only a fraction of them, without altering the quality of the geographical coverage.

When dealing with terrestrial measurements, the first step is to select the quietest measurements (Langel and Hinze, 1998), using routinely computed external activity indices. On Mars, there are no such activity indices. This is the reason why we use a different approach: we compute statistical indices associated with time variations observed for a given location.

Such statistics are computed only for the MO measurements. Measurements are first sorted onto a 0.5°× 0.5° grid. Due to the orbital parameters the altitude remains almost constant over a particular cell, with a maximum amplitude equal to 7.5 km. Second we look for the median value $C_m(c)$ among the N_c observations of each component C in each cell c. The median value is preferred to the mean one as it is less sensitive to possible outliers. Third, a daily index $\sigma_C(d)$ is computed, characterizing the mean perturbation to the median value for each component, based on the N_d measurements acquired for a given day d:

$$\sigma_C^2(t) = \frac{1}{N_d - 1} \sum_{i=1}^{N_d} (C_i(c,d) - C_m(c))^2 \tag{1}$$

where $C_i(c,d)$ is the i^{th} measurement acquired on day d, located in cell c. Indices are computed only for days with more than 100 measurements over the area of interest.

Using this index, measurements are selected on a daily basis, rejecting those acquired on days when the index $\sigma_C(d)$ is higher than a pre-defined value. This value is set to 4 nT, close to the 3 nT estimated accuracy of the MGS measurements (Acuña *et al.*, 1999). For a particular day, all three σ_{Br}, $\sigma_{B\theta}$ and $\sigma_{B\phi}$ have to be lower than 4 nT. The resulting, selected, dataset contains 119198 magnetic vectors. This dataset covers 211 days, which corresponds to one-third of the considered time period. The geographical coverage of the dataset is checked. There are between 65 and 395 measurements for each 1×1° bin.

MO magnetic measurements are plotted on Figure 3. On these maps a clear magnetic signature is found. Both the B_r and B_ϕ components (Figures 3a and

3c) show a change of polarity above the Patera. This change of polarity is aligned on a NW-SE direction. The correlation between the B_θ component (Figure 3b) and the volcano is less evident, even if a (small) local extrema can be noticed about 1 or 2° East of the volcano. However, it has to be noted that the magnetic properties of the area are likely to be complex. Larger anomalies are present on the eastern and southern boundaries as shown by the B map (Figure 3d).

The geographical coverage is far from being complete for the AB-1 data (Figure 2). Only measurements made below 250 km, without any local time consideration, are selected. There are only 3597 measurements, which fill 535 out of 900 cells on a 1°×1° grid. B_r (Figure 2a) changes its polarity above the volcano, on a NW-SE axis. B_θ (Figure 2b) is negative all around the volcano, while B_ϕ (Figure 2c) is positive NE and negative SW of the Patera. There is a local maximum of the magnetic field above the volcano (Figure 2d). These magnetic features are very similar to those measured during the MO phase.

3 Input parameters and modeling approach

Measurements made at different altitudes seem to support a magnetic anomaly that would be associated with a body located below or near the caldera of the Apollinaris Patera. This body could be of various origins, including a magma chamber (Kiefer, 2003). Several modeling approaches could be used, based on different level of complexity for the sources. In the following, we will use a very simple approach, in which the magnetized body(ies) is (are) represented by one (or more) equivalent source dipoles (Purucker *et al.*, 1996). Other methods could have been considered, using vertical prisms, or uniformly magnetized spheres. But these methods require the geometric shape to be *a priori* set or known.

The method we use does not require any geometric information but the location of the point dipole (latitude, longitude and depth). We assume an *a priori* depth of 20 km, following the results of Langlais *et al.* (2004). We assume a 40 km-thick magnetized layer, similar to the one used in previous studies (Purucker *et al.*, 2000; Langlais *et al.*, 2004). The assumed thickness does not affect the results: only the vertically integrated magnetization is actually computed. As a consequence the resulting magnetization is inversely proportional to the assumed thickness. However, we are well aware that this might correspond or not to the depth of the Curie isotherm. This is nevertheless comparable to the mean crustal thickness ($\simeq$50km, Smith and Zuber (2002))

We use several equivalent source dipoles, located homogeneously around the volcano. When dealing with ESD it is important to use a regular mesh (Covington, 1993). Since we are looking at a local problem, located around a spherical edifice, we choose to use a hexagonal mesh. Each equivalent source dipole is located at the center of a hexagon, all hexagons being contiguous. The mean distance between the dipoles is chosen so that it corresponds to the minimum altitude of the data, 110 km above the region of interest. Several meshes are defined, by increasing the number of sources (corresponding to larger areas). Meshes are made of 7, 19, 37, 61, 91, 127 or 169 equidistant sources, respectively. For a given dipole location, only the measurements made within 1500 km of it are used to derive the magnetization components. The 169-dipole mesh is shown on Figure 4.

`Figure 4`

We use a conjugate gradient iterative technique to solve the inverse problem, as done previously in Langlais *et al.* (2004). The relationship between magnetic anomalies and magnetization distribution is non unique. One source of error consists in magnetic annihilators (Parker, 1977), that produce no external field. As a consequence, two different magnetization distributions can produce almost identical magnetic anomalies. This well known feature is enhanced in this study. We consider a very limited area. The further away from the volcano the dipoles are, the more they are to be influenced by other magnetic anomalies. It is thus very important to define criteria by which a simple solution consistent with the observations can be defined. First, the evolution of the root mean square differences between the measurements and the model predictions are examined between successive iterations. This is done over a limited area, in order to avoid edge effects. Second, the convergence of the solution is investigated, by comparing the changes between magnetic field predictions and magnetization distribution. Third, the evolution of the root mean square value of the magnetization intensity (regardless of the direction) is compared to the evolution of root mean square residuals. This scheme allows us to retain only one solution for a given dipole mesh.

4 Results

We start with the single dipole case. We determine what is the most likely location of the paleopole associated with this single-dipole solution. We then consider multiple-dipole cases, first using the paleopole to impose magnetization directions, and second without any assumption on the magnetization directions.

4.1 Using a single dipole

We first test the coherency of the low-altitude, sparse AB-1 measurements with the high-altitude, homogeneously located MO measurements. A single dipole is located at -8.75° S, 174.50° E, the position of the maximum gravity anomaly. We first look for the dipole directions and magnetization, using either the AB-1 or MO measurements. Both approaches give similar results. The dipole inclination is -8.41° and 2.54° for the AB- and MO-based models, respectively, while the declination is found to be -157.40° and -157.81°. Associated paleopoles are located -64.00°N, 55.44°E and -66.68°N, 67.03°E, respectively.

The magnetization directions and intensity are then solved for using AB and MO measurements together. Several dipole locations are tested, on a $1/4 \times 1/4°$ grid of a $1 \times 1°$ side square, centered on the volcano. For each location, the dipole is assumed to be located 20 km below the mean surface, following the conclusions of Langlais *et al.* (2004). All 25 models give similar results in terms of inclination and declination. The inclination ranges from -13.72 to 4.87°, while the declination ranges from -160.22 to -155.90°. The mean position of the paleopoles is 65.06°S, 59.44°E.

It is unfortunately impossible to estimate what is the exact location of the magnetic source. Rms differences between measurements and predictions based on a particular dipole are indeed biased by the poorer geographical distribution of the AB measurements. Less measurements lead to apparently better fit to the data. However, assuming that the magnetic anomaly can be modeled by a single dipole, located on or near Apollinaris Patera, then its magnetized vector is almost horizontal, pointing towards the South.

4.2 Using more than one equivalent source dipole

When considering magnetic measurements acquired on or above a topographic elevation on the Earth, we generally refer to the seamount problem (Vacquier, 1972; Parker *et al.*, 1987). This approach usually relies on marine survey measurements, acquired over small-scale structures (a few tens of kilometers). The simplest case is associated with uniform magnetization. This is appropriate when dealing with small edifices, that were put in place relatively quickly. For recent structures, the magnetization direction can be approximated, and aligned onto the main magnetic field. In this case, a uniform magnetization over the whole volume is assumed. Only the magnetization moment is solved for.

For more complex or older edifices, one has to consider possible non uniform magnetization (Parker *et al.*, 1987). This can be due for instance to the evolution of the magnetic field between initial and final eruptive events, or to an evolution of the magnetic mineralogy. It is generally assumed that the duration of the seamount volcanism is long enough to average out the effects of the secular variation. But it can also be long enough to experience one or more field reversals. In this case, and assuming that the magnetic axis remained similar, two or more opposite magnetic layers will produce less intense magnetic anomalies, by canceling one each other. In this case, only the apparent magnetization moment is solved for. The worst scenario would correspond to almost equally thick magnetic layers, resulting in an almost null magnetization. Exactly equally thick layers would indeed not cancel each others, the upper one being closer to the sources than the bottom one.

The period over which Apollinaris Patera was active likely extends 10^7 years (Robinson *et al.*, 1993). Assuming there was an internal magnetic field at this time (similar to the terrestrial one), its rapid fluctuations can safely be ignored during this long interval, and only the mean direction of the dipolar field can be assumed to be constant. However a field reversal can not be excluded. Similarly, a magnetic axis wander can not be ruled out. In order to investigate such possibilities, two cases are studied. First, we consider an uniform magnetization for the whole area. Second, we let the magnetization direction vary around the volcano.

4.2.1 Uniform magnetization case

First we consider the uniform magnetization case. The direction of the magnetization is assumed to be fixed with respect on a mean paleopole position. Since both inclination and declination previously computed are very consistent, whatever the altitude of the used measurements (AB or MO), or the exact location of the dipole (inside a 1° square around the volcano), the considered paleopole is the one computed using the single dipole solution, leading to (65.06°S, 59.44°E).

Corresponding input declination and inclination for the 7-dipole grid range between -157.88 and -157.20° and between -8.03 and -0.78°, respectively. For the 169-dipole grid, inclination ranges between -28.08 and 20.40° while declination ranges between -160.44 and -155.41°.

The rms residuals between measurements and model prediction decrease as the iteration number increase. They also decrease as more sources are used. The value of the residuals is however controlled by the intense magnetic anomalies located to the SW and to the East of the area (see Figure 4). This is why we consider the evolution of the residuals over a limited area, surrounding the volcano. Similarly the magnetization of the outer sources is influenced by these intense anomalies, in addition to edge effects. Thus the magnetization of these dipoles can not be considered as reliable. In the following, rms residuals will refer to residuals computed within 2.5° of the volcano for the MO measurements. AB rms residuals are meaningless as less than 100 measurements are located within 2.5° of the volcano. We however visually check the residuals.

`Figure 5`

The first step is to select a model for each dipole mesh. In each case we stopped the iterations when the residuals no longer decreased significantly when compared to the increase of the rms magnetization. Then the evolution of the rms residuals is compared to the number of sources. A minimum is reached for 127 sources, or 6 concentric hexagons (Figure 5). The final model corresponds to the 10th iteration. Locally, rms residuals are as low as 3.16 nT. The difference between 127- and 169-dipole mesh is very small. Associated magnetic field predictions are show on Figure 6 and 7 for the AB and MO measurements, respectively. Predictions are very close to the actual measurements. In particular, the change of sign of the B_r component is well reproduced. The poorest predictions are associated with the B_ϕ component, where external fields are probably largest.

Figure 6

Figure 7

We show on Figure 8 the magnetization distribution associated with the 127-dipole mesh solution. Both positive and negative magnetizations are plotted. A negative value is associated with a magnetization acquired in a reversed field (assuming that the central one was acquired in a normal field). It is interesting to note that the magnetization does not present any change of sign above and around the volcano. This is very important, as this means that the magnetization associated with the volcano has a single polarity. The behavior of the more remote sources (starting with the 3rd hexagon) is controlled by edge effects. The magnetization of the 7 central sources range between 0.2 and 10.1 A/m (for a 40-km thick layer). These values are comparable to the ones given in previous studies (Parker, 2003; Langlais *et al.*, 2004).

Figure 8

4.2.2 Non uniform magnetization case

In order to *a posteriori* check this result, we also study the non uniform magnetization case. We do not make any assumption on the direction of the magnetization. We do not impose any spatial coherency. This corresponds to solving for (M, D, I). We apply the same procedure as for the uniform magnetization case. We first look for the best solution is terms of local rms residuals for each dipole mesh, and then determine what appears to be the best dipole mesh. The 7-dipole mesh leads to lower rms residuals than the 19-dipole mesh (Figure 9). However, this solution is not satisfactory in terms of predicting the AB measurements. We disregarded it, and retain the 61-dipole solution. It corresponds to the 10th iteration. The magnetic field (local) predictions associated with this model are very similar to the ones by the coherent 127-dipole mesh, even if this solution offers a slightly better fit (2.81 nT). We plot on Figure 10 the magnetization components M, I and D. Again, negative values for M correspond to magnetizations acquired in a reversed field when compared to the one of the central dipole. A paleopole location is computed for each equivalent source dipole. We show on Figure 11 the location of the paleopoles associated with the 7 closest dipoles. Their spatial distribution shows a clustering, around the South Pole. The mean paleopole position is (87.8°S, 99.2°E).

`Figure 9`

`Figure 10`

`Figure 11`

This mean location was checked using other dipole meshes. We looked for the mean paleopole location associated with the 7 closest sources of the best solution. For 37 and more dipoles, the mean paleopole is always South of 80°S.

This clustering of the paleopoles confirms the results of the uniform magnetization case. The magnetic field measured above Apollinaris Patera is coherent with a horizontal magnetization pointing South. If one assumes that this magnetization was acquired at the time when the volcano was set into place, then this would mean that little or no polar wander has occurred since this epoch.

5 Discussion

In this paper, we examine a magnetic anomaly associated with a relatively large and isolated volcanic edifice. This is the first study in which a magnetic anomaly is clearly associated with a geologic feature, other than the negative association with impact features first recognized by Acuña *et al.* (1999). There is a coincident gravity anomaly, which may originate as a high-density magma chamber under the volcano (Kiefer, 2003). By virtue of the density contrast with its surroundings, we infer that this magma chamber is iron-rich. It is very likely that this iron-rich material contributes significantly to the magnetic anomaly. This association allows for a more accurate determination of a paleomagnetic pole (Parker *et al.*, 1987) than previously possible on Mars.

Both low- and high-altitude measurements are considered. Given the numerous MO measurements, it is possible to make a selection with respect to external perturbations, but still consistent with complete geographical coverage. We estimate a daily activity index, and kept only measurements acquired during the quietest days. External fields were also modeled and removed. The results did not change significantly. We also simulated a central demagnetization, associated to the latest stages of the volcanic activity. Taking a Curie temperature of 500°C or so, a lava temperature of 1200°C and a thermal gradient of 30°/km, then an area of 23 km (radius) would be affected. Taking a conservative approach corresponds to remove the central dipole. Magnetization distribution, magnetic field predictions and paleopole clustering do not change.

Low- and high-altitude measurements are coherent and show similar patterns. The inverse problem is formulated using an equivalent source dipole approach, which is a simple but effective space domain technique. Two cases are investigated. First, we assume an *a priori* uniform magnetization direction, fixed with respect to a magnetic paleopole. The location of this paleopole is estimated by fitting the measurements with only one dipole located below the volcano. The best solution is made of 127 sources, located homogeneously around the volcano. The magnetization signature of the closest sources is spatially coherent. No field reversal is recorded by the volcanic edifice. This does not mean that the Martian dynamo did not experience any reversals.

Second we do not assume any *a priori* magnetization directions. In this case the best solution consists of 61 dipoles. The directions we find do not differ much from the uniform case. Paleopoles associated with the closest sources cluster around (87.8°S, 99.2°E). We apply to this results paleomagnetic statistics. Paleomagnetic studies typically rely on tens of samples collected at the same location. The confidence of the results is usually described by the α_{95} parameter. It corresponds to the 95% confidence interval (Butler, 1992). Here we have to deal with 7 directions, located at different locations. We first correct the magnetization directions for the location differences. We find a $\alpha 95$ equal to 18.98°. For a terrestrial study, this would be considered as a high value. But we have to deal here with a very large edifice. We can compare it to larger scale studies on the Earth. Typical dispersion of paleopoles associated with equatorial sources is of the order of 13° (Merrill *et al.*, 1996). This is very close to what we observe in this study.

We compare this result to previous studies. The magnetization model of Whaler and Purucker (2005) predicts a substantial magnetization anomaly (2 A/m over a 40 km thick crust) almost coincident with the gravity anomaly. The paleomagnetic pole associated with a source at the location of the maximum gravity anomaly would be located at 79.3°S, 85.8°E. The magnetization model of Langlais *et al.* (2004) predicts a magnetization anomaly of comparable extent and magnitude, and the paleomagnetic pole evaluated at a source interpolated at the maximum gravity anomaly would be located at 66.51°S, 31.62°E.

Based on crater counts, Apollinaris Patera seems to be younger than Hellas and Argyre impact craters. However, there exist other martian volcanoes which activity has been intermittent over billions of years. The observed magnetic anomaly could signify that the Patera is actually older than the oldest visible surface.

This new result however differs from studies based on isolated magnetic anomalies (Frawley and Taylor, 2004; Arkani-Hamed and Boutin, 2004). It is possible to reconciliate these different results: the Martian dynamo likely experienced a complex history, including field reversals. Polar wander is also possible, linked to the rise of the Tharsis bulge (Sprenke *et al.*, 2005). Another volcano with a gravity (Kiefer, 2003) and magnetic (Whaler and Purucker, 2005) signature is Tyrrhena Patera, located NE of Hellas. These signatures are broader, and more complicated, than those at Apollinaris Patera, as befitting a much more extensive volcanic complex. It remains to be seen whether reliable paleomagnetic pole information can be extracted from this volcano, and if it confirms the present study.

Acknowledgements

Authors wish to thank an anonymous reviewer for his constructive critiques. Part of this study was performed while B.L. was supported by a NAS/NRC postdoctoral fellowship and while M.E.P. was in residence as Visiting Professor at the University of Nantes, France. This research benefited from the support of the European Community's Improving Human Potential Programme under contract RTN2-2001-00414, MAGE.

References

Acuña, M.H., Connerney, J.E.P., Ness, N.F., Lin, R.P., Mitchell, D., Carlson, C.W., McFadden, J., Anderson, K.A., Rème, H., Mazelle, C., Vignes, D., Wasilewski, P., and Cloutier, P., 1999. Global distribution of crustal magnetization discovered by the Mars Global Surveyor MAG/ER experiment. Science, 284, 790-793.

Albee, A.L., Arvidson, R.E., Palluconi, F., and Thorpe, T., 2001. Overview of the Mars Global Surveyor Mission. J. Geophys. Res., 106, 23291-23316.

Arkani-Hamed, J., 2001. Paleomagnetic pole positions and pole reversals of Mars. Geophys. Res. Lett., 28, 3409-3412.

Arkani-Hamed, J., 2002. Magnetization of the Martian crust. J. Geophys. Res., 107,doi:10.1029/2001JE001496.

Arkani-Hamed, J.,2004. A coherent model of the crustal magnetic field of Mars. J. Geophys. Res., 109, doi:10.1029/2004JE002265.

Arkani-Hamed, J., and Boutin, D., 2004. Paleomagnetic poles of Mars: Revisited. J. Geophys. Res., 109, doi: 10.1029/2003JE002229.

Butler, R.F., 1992. Paleomagnetism. Blackwell Sci., Malden, Mass.

Cain, J.C., Ferguson, B.B., and Mozoni, D., 2003. An n=90 internal potential function of the Martian crustal magnetic field. J. Geophys. Res., 108, doi:10.1029/2000JE001487.

Connerney, J.E.P., Acuña, M.H, Wasilewski, P.J., Ness, N.F., Rème, H., Mazelle, C., Vignes, D., Lin, R.P., Mitchell, D., and Cloutier, P., 1999. Magnetic lineations in the ancient crust of Mars. Science, 284, 794-798.

Connerney, J.E.P., Acuña, M.H., Wasilewski, P.J., Kletetschka, G., Ness, N.F., Rème, H., Lin, R.P., and Mitchell, D., 2001. The Global Magnetic Field of Mars and Implications for Crustal Evolution, Geophys. Res. Lett., 28, doi:10.1029/2001GL013619.

Connerney, J.E.P., Ness, N.F., Spohn, T., and Schubert, G., 2004. Mars Crustal Magnetism. Space Sci. Rev., 111, 1-32.

Covington, J., 1993. Improvement of equivalent source inversion technique with a more symmetric dipole distribution model. Phys. Earth and Plan. Int., 76, 199-208.

Frawley, J.J., Taylor, P.T., 2004. Paleo-pole positions from martian magnetic anomaly data. Icarus 172, 316-327.

Frey, H.V., 2004. A timescale for major events in early Mars crustal evolution. Lunar and Planetary Science Conf. XXXV, Abstract 1382.

Gauss, C.F., 1839. Allgemeine Theorie des Erdmagnetismus. In Resultate aus den Beobachtungen des magnetischen Verein im Jahre 1838, 1-52, Leipzig, Göttingen Magn. Ver., Germany.

Hood, L.L., and Zakharian, A., 2001. Mapping and modeling of magnetic anomalies in the Northern polar region of Mars. J. Geophys. Res., 106, 14601-14619.

Hood, L.L., Richmond, N.C., Pierazzo, E., and Rochette, P., 2003. Distribution of crustal magnetic fields on Mars: Shock effects of basin forming impacts. Geophys. Res. Lett., 30, doi:10.1029/2002GL016657.

Kiefer, W.S., 2003. Gravity evidence for extinct magma chambers on Mars: Tyrrhena Patera and Hadriaca Patera. Lunar and Planetary Science Conf. XXXIV, Abstract 1234.

Langel, R.A., and Hinze, W.J., 1998. The magnetic field of the earth's lithosphere, the satellite perspective. Cambridge University Press, 430 pp.

Langlais, B., Purucker, M.E., and Mandea, M., 2004. The crustal magnetic field of Mars. J. Geophys. Res., 109, doi:10.1029/2003JE002058.

Lemoine, F.J., Smith, D.E., Rowlands, D.D., Zuber, M.T., Neumann, G.A., Chinn, D.S., and Pavlis, D.E., 2001. An improved solution of the gravity field of Mars (GMM-2B) from Mars Global Surveyor. J. Geophys. Res., 106, 23359-23376.

Maus, S., Rother, M., Holme, R., Lühr, H., Olsen, N., and Haak, V., 2002. First scalar magnetic anomaly map from CHAMP satellite data indicates weak lithospheric field. Geophys. Res. Lett., 29, doi:10.1029/2001GL013685.

Melosh, H.J., 1980. Tectonic patterns on a reoriented planet-Mars. Icarus, 44, 745-751.

Merril, R.T., McElhinny, M.W., and McFadden, P.L., 1996. The Magnetic Field of the Earth. Int. Geophys. Ser., vol. 63, 531 pp., Academic, San Diego, Calif..

Nimmo, F., and Gilmore, M.S., 2001. Constraints on the depth of magnetized crust on Mars from impact craters. J. Geophys. Res., 106, 12315-12323.

Parker, R.L., 1977. Understanding Inverse Theory. Annu. Rev. Earth Planet. Sci., 5, 35-64.

Parker, R.L., Shure, L., and Hildebrand, J.A, 1987. The application of inverse theory to seamount magnetism. Rev. Geophys., 25, 17-40.

Parker, R.L., 2003. Ideal bodies for Mars magnetics. J. Geophys. Res., 108, doi:10.1029/2001JE001760.

Purucker, M.E., Sabaka, T.J., and Langel, R.A., 1996. Conjugate gradient analysis: a new tool for studying satellite magnetic data sets. Geophys. Res. Lett., 23, 507-510.

Purucker, M.E., Ravat, D., Frey, H., Voorhies, C., Sabaka, T., and Acuña, M., 2000. An altitude-normalized magnetic map of Mars and its interpretation. Geophys. Res. Lett., 27, 2449-2452.

Robinson, M.S., Mouginis-Mark, P.J., Zimbelman, J.R., Wu, S.S.C., Ablin, K.K., and Howington-Kraus, A.E., 1993. Chronology, eruption duration, and atmospheric contribution of the martian volcano Apollinaris Patera. Icarus, 104, 301-323.

Schubert, G., Russel, C.T., and Moore, W.B., 2000. Timing of the Martian dynamo. Nature, 408, 666-667.

Smith, D.E., and Zuber, M.T, 2002. The crustal thickness of Mars: accuracy and resolution. Lunar Planet. Sci. Conf., XXXIII, Abstract 1893.

Sprenke, K.F., Baker, L.L., and Williams, A.F., 2005. Polar wander on Mars: Evidence in the geoid. Icarus, 174, 486-489.

Stevenson, D.J., 2001. Mars' core and magnetism. Nature, 412, 214-219.

Vacquier, V., 1972. Geomagnetism in Marine Geology. Elsevier Publishing, Amsterdam, 185pp.

Werner, S.C., 2005. Major Aspects of the Chronostratigraphy and Geologic Evolutionary History of Mars. PhD thesis, Freie Universität Berlin.

Whaler, K.A., and Purucker, M.E., 2005. A spatially continuous magnetization model for Mars. J. Geophys. Res., 110, doi:10.1029/2004JE002393.

Zuber, M.T., 2001. The crust and mantle of Mars. Nature, 412, 220-227.

Figure 1 - (a) Topography around Apollinaris Patera, and (b) associated gravity anomaly, from Lemoine *et al.* (2001).

Figure 2 - Magnetic measurements acquired near Apollinaris Patera during the AB-1 phase below 250 km altitude: (a) B_r; (b) B_θ; (c) B_ϕ; (d) B. No altitude correction is applied. Orbits are superposed onto a shaded relief.

Figure 3 - Magnetic measurements acquired near Apollinaris Patera during the MO phase between 370 and 395 km altitude: (a) B_r; (b) B_θ; (c) B_ϕ; (d) B. Iso-contours are plotted every 10 nT. Dashed lines correspond to negative values. Orbits are superposed onto a shaded relief.

Figure 4 - Hexagonal dipole mesh. There are 169 sources, the mean distance is 116 km.

Figure 5 - Rms residuals between MO measurements and coherent-model predictions with respect to the number of sources. Only measurements within 2.5° of the volcano are taken into account.

Figure 6 - Magnetic field predictions associated with the 127-dipole coherent model: (a) B_r; (b) B_θ; (c) B_ϕ; (d) B. Predictions are made at AB-1 measurement locations.

Figure 7 - Magnetic field predictions associated with the 127-dipole coherent model: (a) B_r; (b) B_θ; (c) B_ϕ; (d) B. Predictions are made at MO measurement locations.

Figure 8 - Magnetization distribution associated with the 127-dipole coherent model. An a priori paleopole is assumed. Negative magnetizations correspond to anomalies acquired in a reversed field.

Figure 9 - Rms residuals between MO measurements and model predictions with respect to the number of sources. No a priori assumptions on magnetization directions. Only measurements within 2.5° of the volcano are taken into account.

Figure 10 - Magnetization distribution associated with the 61-dipole mesh: (a) M; (b) I; (c) D. No a priori assumption on the paleopole location. Negative magnetizations correspond to anomalies acquired in a reversed field.

Figure 11 - Paleopole locations associated with the 61-dipole mesh. Only the closest dipoles are taken into account. Black diamond corresponds to the central dipole. White diamonds correspond to the first hexagon. White star corresponds to the paleopole associated with the 127-dipole coherent model.

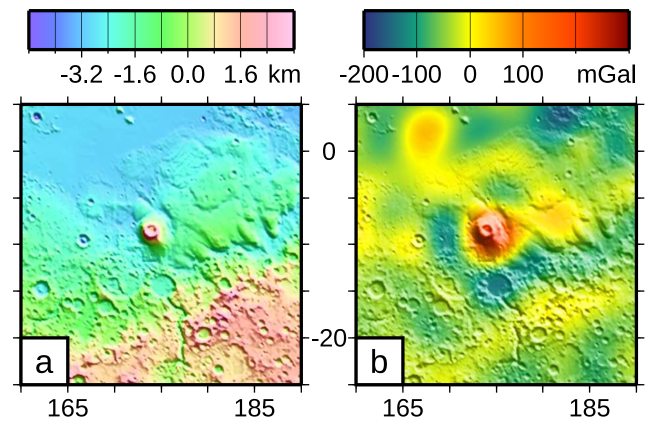

-3.2 -1.6 0.0 1.6 km
-200 -100 0 100 mGal
0
-20
a
b
165
185
165
185

Fig. 1.

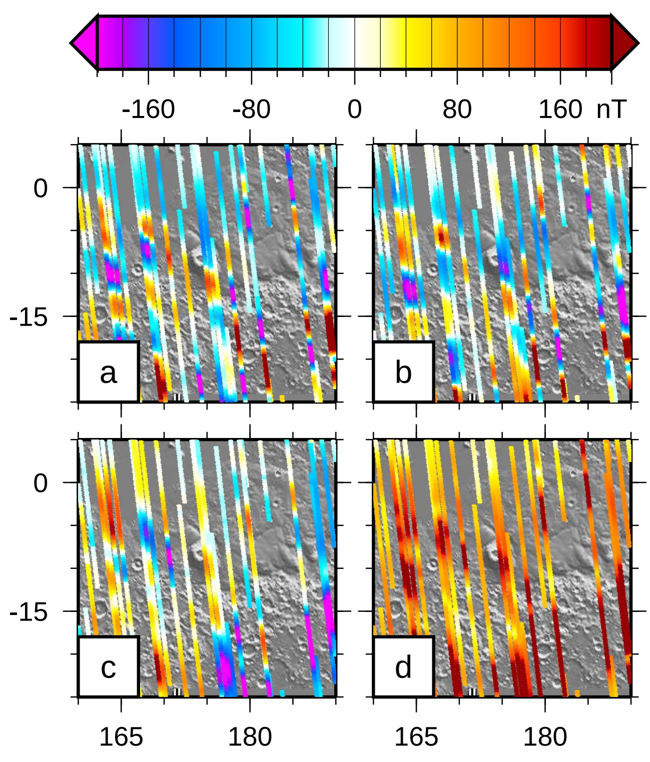

-160 -80 0 80 160 nT
0
-15
a
b
c
d
165
180
165
180

Fig. 2.

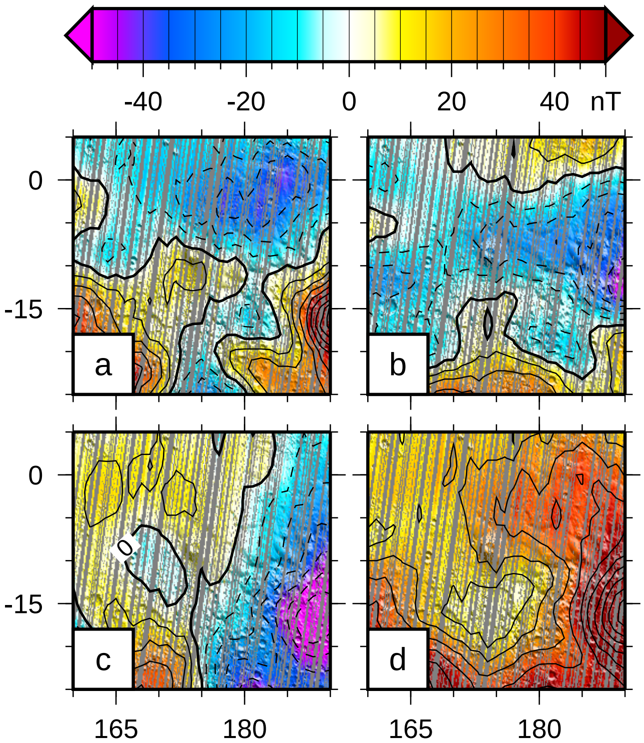

Fig. 3.

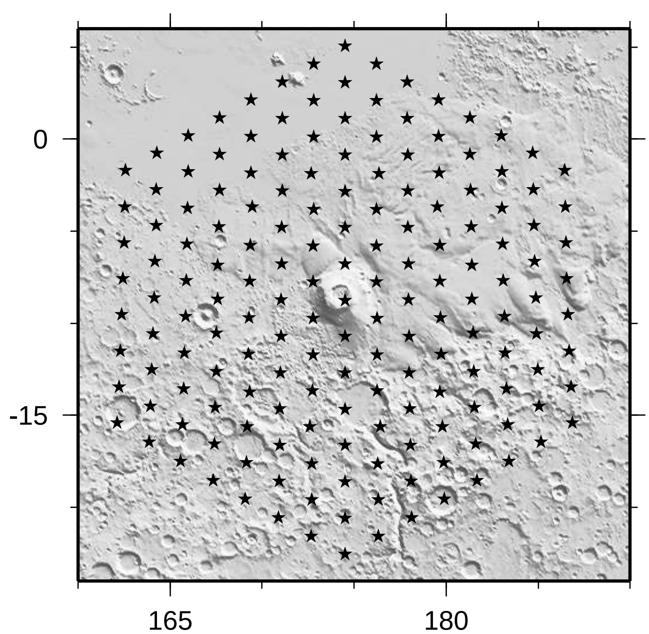

Fig. 4.

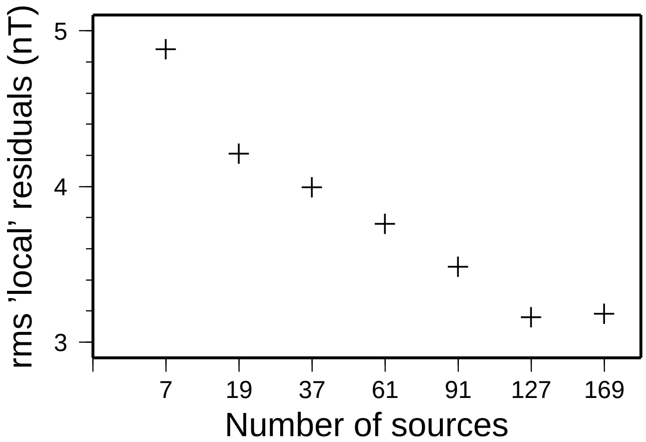
rms 'local' residuals (nT)
5
4
3
7
19
37
61
91
127
169
Number of sources

Fig. 5.

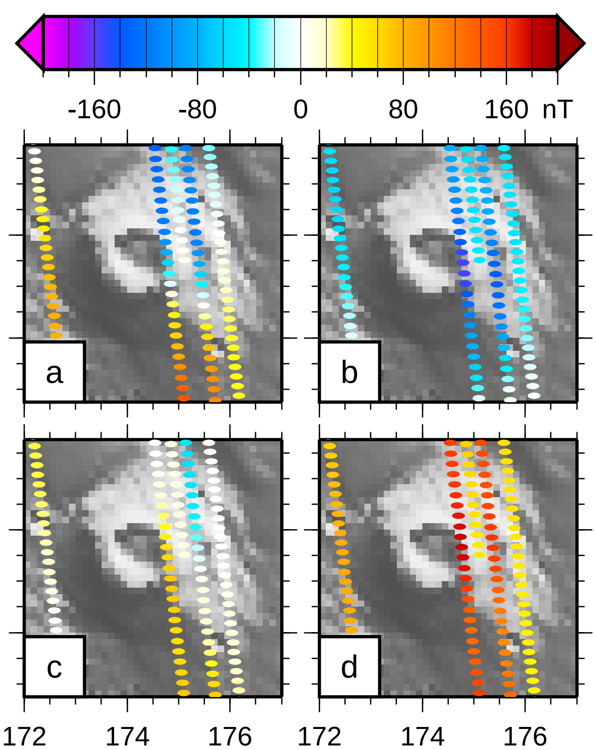
-160
-80
0
80
160
nT
-8
-10
a
b
c
d
172
174
176
172
174
176

Fig. 6.

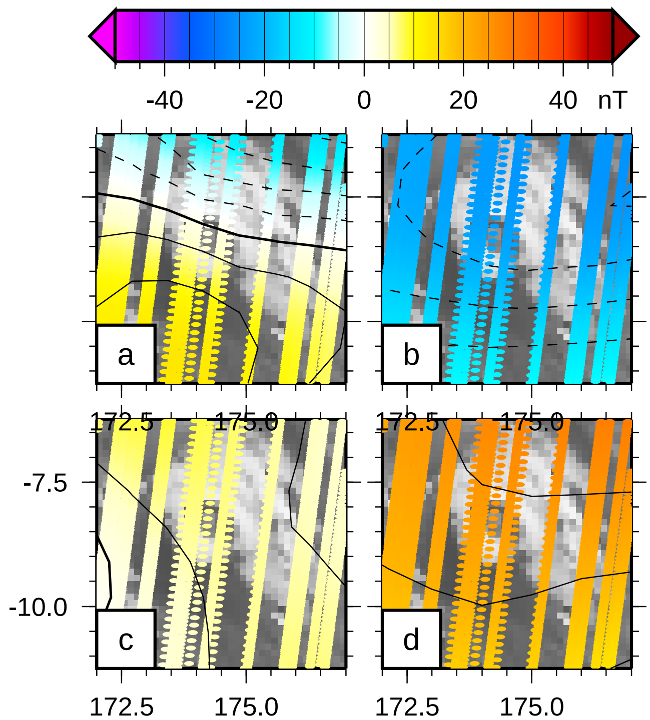

Fig. 7.

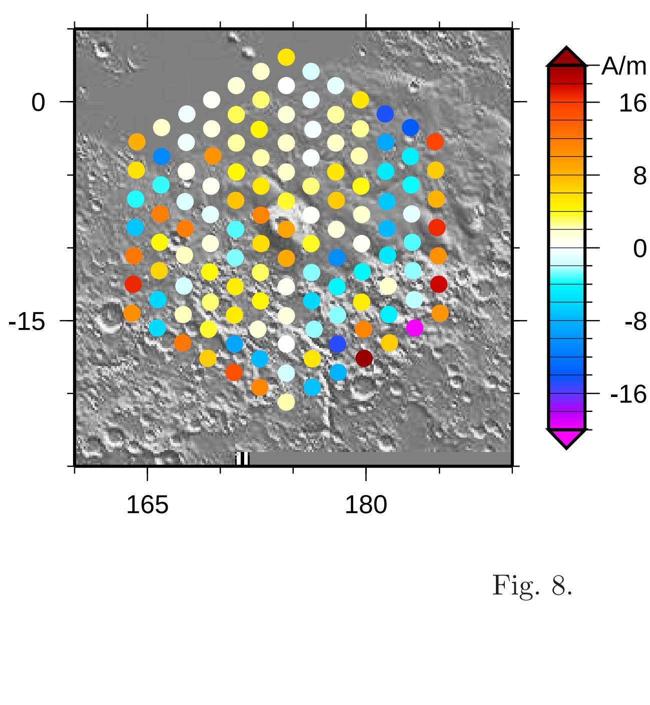

Fig. 8.

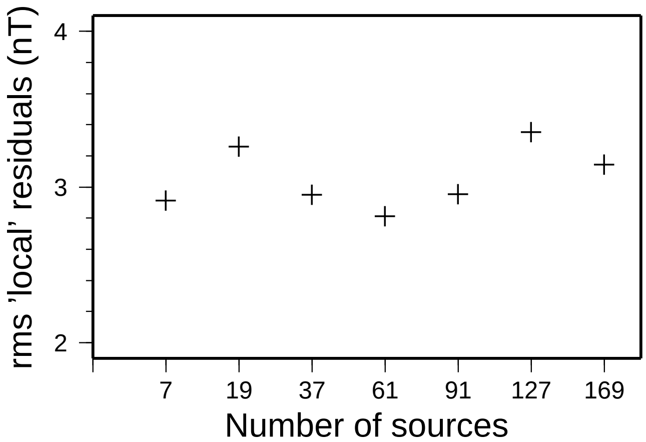
rms 'local' residuals (nT)
4
3
2
7
19
37
61
91
127
169
Number of sources

Fig. 9.

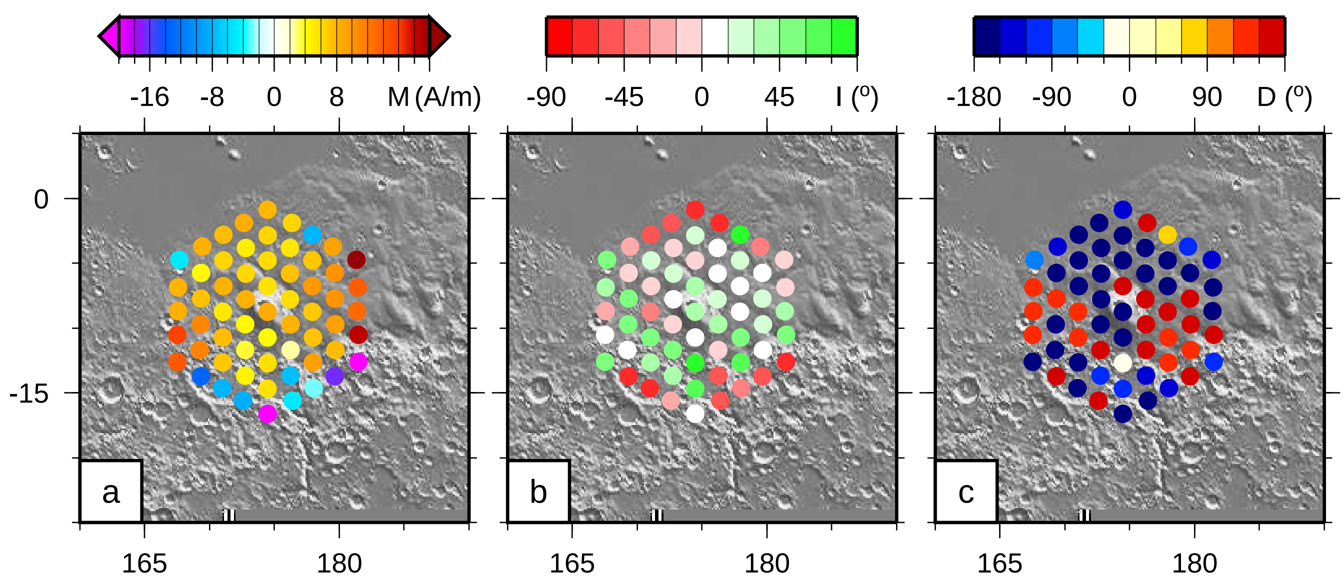
-16
-8
0
8
M (A/m)
-90
-45
0
45
I (°)
-180
-90
0
90
D (°)
0
-15
165
180
a
b
c

Fig. 10.

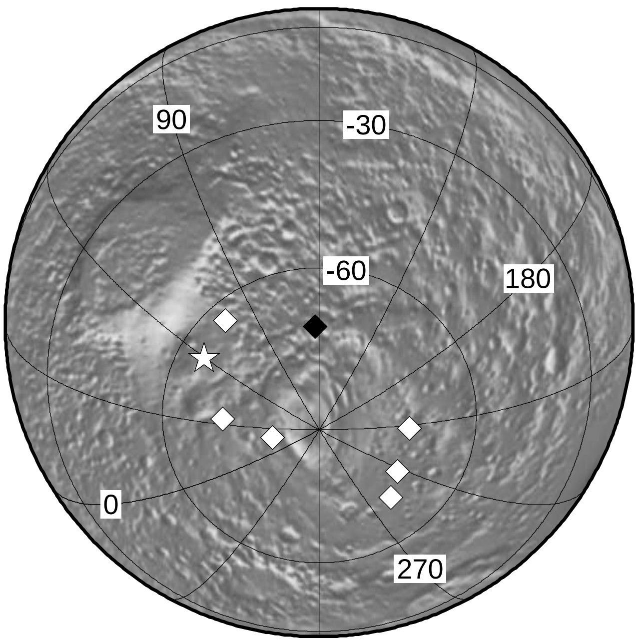

Fig. 11.